Spatial Instabilities in the Regeneration of Diesel-Particulate Filters

An instability is proposed that can lead to channel formation during the regeneration of monolithic diesel-particulate filters. This instability, which occurs during the transport-controlled combustion of the soot bed, is compared to a kinetically driven instability by using a numerical model for channel growth. Both mechanisms are shown to be important and may lead to higher thermal stresses in the filter wall. It is suggested that both mechanisms can be controlled by the ratio of the filter-plate to soot-bed flow resistance, lateral heat transfer, and other design parameters.

James H. Saunders, Jr.
Battelle
Columbus, OH 43201

Introduction

Diesel-particulate filters, or trap oxidizers, are under development to reduce particulate emissions from diesel vehicles to the levels required in the 1990s. One of the most promising devices, the wall-flow monolithic filter, collects soot on a honeycomb network of porous ceramic channels located in the engine exhaust stream (Wade et al., 1983; MacDonald and Simon, 1988). The channels are open at one end and closed at the other. Half of the channels—the inlet channels—have their open ends facing upstream; the other half, adjacent to these, have their open ends facing downstream. In this manner, exhaust gas enters an inlet channel, flows through the porous channel walls, and exits through the adjacent channel, as illustrated in Figure 1. Consequently a thin, porous soot bed is formed on the inside wall of the inlet channel as the gas passes through the wall. Once a sufficient mass of particles is collected, it is burned off to regenerate the filter bed by heating the exhaust gas with either a small burner or an engine control method. Controlling this regeneration process is an active and critical area of diesel research and development, since overheating during the regeneration process can result in a structural failure of the filter. In addition, excessive filter pressure drop, caused by infrequent regeneration, can reduce engine fuel economy and performance.

Previous workers have shown that the regeneration process sometimes occurs more rapidly in localized areas in the filter. Wiedemann et al. (1983, 1984) suggested that an instability can exist which leads to spatially nonuniform burning of the soot bed and the formation of channels in the soot. In this paper, an additional spatial instability mechanism is proposed, and the relationship between the two is explored with a simple numerical model. Both mechanisms may exist during typical regeneration processes, resulting in longer regeneration times than for a uniformly regenerating filter and, perhaps more significantly, hot and cool spots on the filter plate that cause higher thermal stresses. These stresses may vary in location and magnitude from one regeneration cycle to the next since the channel formation is dependent upon the shape of the bed surface prior to regeneration. Indeed, experiments have suggested that these localized patterns seem to vary randomly in successive cycles (Montierth, 1984). To illustrate the mechanisms in their simplest form, idealized mathematical and numerical models are presented for limiting cases that retain only essential parameters. The regeneration process in an actual filter is considerably more complex; therefore experiments and more detailed models must be used to predict actual system behavior. Results suggest that controlling the ratio of filter-plate pressure drop to soot-bed pressure drop can control the growth rate of certain spatial nonuniformities, and estimates are given for the values of this ratio that can limit growth. The mechanisms are somewhat analogous to the morphological instabilities that can occur during phase transitions, such as in crystal growth (Langer, 1980). These instabilities have also been proposed in the combustion of isolated spherical particles (McGraw and Wegrzyn, 1985). Somewhat similar tendencies to channeling in fluidized beds have been studied by Siegel (1976) and in ice counterwashers by Grossman (1976).

Mathematical models of the thermal regeneration process have been developed previously (Wiedemann et al., 1983, 1984; Bissett, 1984; Bissett and Shadman, 1985). Bissett and Shadman considered the one-dimensional flow of a gas down through a uniform soot bed resting upon a porous plate. They showed that the regeneration occurs in four stages: preheat, ignition, transport-controlled combustion, and cooldown, with significant soot combustion occurring in the second and third stages. This

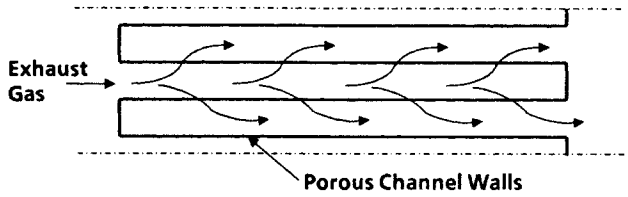

Figure 1. Flow passages in a monolithic wall-flow filter.

can be seen in the equation for the rate of removal of soot from the bed, assuming first-order oxidation of carbon to CO_2:

$$\frac{dh}{dt} = -\frac{M_c \rho}{M_a \rho_b}(y_i - y_e)u + \frac{f}{\rho_b} \tag{1}$$

(See the Notation for definition of variables.) During the ignition stage, the oxygen mole fraction at the bed exit, y_e, is greater than zero, while during transport-controlled combustion $y_e = 0$ and the burning rate is controlled by the flow of oxygen to the bed, $y_i u$. Solving the equations by an interesting perturbation technique, Bissett and Shadman found that, to first order, the bed temperature profile was essentially uniform at each instant in time for the parameter values they considered.

Wiedemann et al. (1983, 1984) suggested that spatially nonuniform burning starts in regions where the bed is thickest. Here the flow resistance is highest and the gas flow is retarded, resulting in less energy being convected away from the bed, and therefore earlier ignition. The thicker bed area completes regeneration first, leaving the thinner regions behind.

However, during the transport stage of the combustion process an increase in local gas velocity can result in a faster rate of combustion. This is the basis of the mechanism presented in this paper. This instability is quite different from the previous one: thinner bed areas complete regeneration first, leaving the thicker regions behind.

In the following sections a simple analysis is presented illustrating the transport-controlled instability and the salient parameters. Next a numerical model is developed and used to show that both instability mechanisms can be important and to explore the relationship between them. Finally, examples are presented in which the design parameters cause the two instabilities to complement each other, leading to large channel growth.

Transport-Controlled Instability

Consider a thin soot bed supported by a porous plate with a depression momentarily created on the bed surface, Figure 2. For now consider the depression to be formed during the transport stage. Additional flow will be diverted to this incipient channel if the pressure drop through the reduced bed thickness is less than through the undisturbed surface. The additional flow of oxygen will increase the burning rate in the channel, promoting channel formation, which diverts more flow to the channel, causing it to grow further. Consequently, less flow then goes through the undisturbed surface, slowing its burning rate.

An assumption in this scenario is that the interparticle forces are strong enough that the particles are locked into a homogeneous, porous structure and are not able to fill in the channel. This is likely to be true for small particles, such as diesel soot,

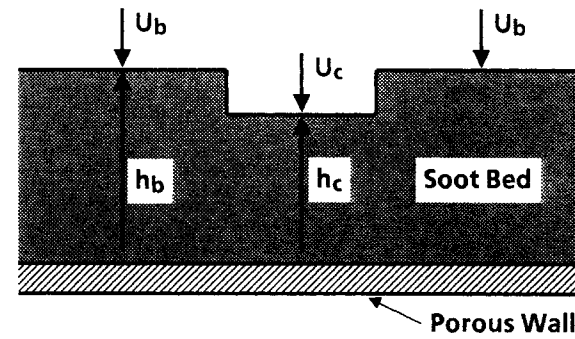

Figure 2. Channel formation in regenerating soot bed.

where interparticle forces are stronger than fluid and gravity forces.

To estimate the significance of channel formation on the burning time of the bed, a one-dimensional calculation is made by assuming the channel remains rectangular, as shown in Figure 2; that is, we neglect pressure gradients and flows parallel to the filter wall. In addition, we assume that the burning rate is much faster than the soot deposition rate and that deposition may be neglected. The gas is assumed to adjust its direction relative to the prevailing flow resistances much faster than the time required for the bed height to significantly change, and the gas-phase pressure gradients are neglected in comparison to pressure gradients through the bed. We assume that velocity and permeability do not change appreciably through the bed thickness and that average values may be used. We also assume a linear dependence of pressure drop on velocity in both the bed and porous wall. The analysis can of course be repeated with different ΔP-u functional forms. Because of the nearly uniform temperature field reported in Bissett and Shadman (1985), we initially neglect the difference in temperature between the bed and channel. Later, in the numerical model, this assumption will be relaxed. To examine the effect of channel formation on burnout time we assume that the instantaneous pressure drop through the bed and porous plate is

$$\Delta P = (R + h\delta)u \tag{2}$$

Here the first term on the righthand side of Eq. 2 denotes the porous wall flow resistance, and the second term denotes the bed resistance.

During the transport stage, Eq. 1 for the undisturbed bed (hereafter referred to simply as the bed) is:

$$\frac{dh_b}{dt} = -Bu_b \tag{3}$$

where $B = (M_c \rho / M_a \rho_b) y_i$, and for the channel:

$$\frac{dh_c}{dt} = -Bu_c \tag{4}$$

The continuity equation is:

$$\alpha u_c + (1 - \alpha)u_b = u \tag{5}$$

where α is the fraction of bed area occupied by the channel. Sub-

stituting Eqs. 3 and 4 into Eq. 5 and rearranging gives:

$$(1-\alpha)\frac{dh_b}{dt}+\alpha\frac{dh_c}{dt}=-Bu \tag{6}$$

The lefthand side is the rate of change of the average bed height, which is receding at the rate $-Bu$, the recession rate of an unperturbed bed surface. Consequently, with these approximations we expect no effect of channel formation on burnout time until h_c reaches zero. At this point the channel has burned through to the porous wall, and the flow through the channel no longer contributes to burning the particles. Furthermore, it is after this point that larger thermal stresses are expected in the wall, since the exhaust gas passes thorugh the channel and wall without reacting, locally cooling the wall. Consequently, wall stress patterns might develop that would not exist in a uniformly burning bed, and these patterns may vary from one regeneration cycle to the next.

Therefore, only after $h_c = 0$ does the burning time increase. So as a first approximation, we seek the wall flow resistance, R, that will keep h_b/W small when $h_c = 0$. This is easily derived by dividing Eq. 4 by Eq. 3, using Eq. 2 and assuming that the pressure drops through the bed and channel are equal:

$$\frac{dh_c}{dh_b}=\frac{u_c}{u_b}=\frac{(R+\delta h_b)}{(R+\delta h_c)} \tag{7}$$

with the initial condition $h_b - h_c = d$ when $h_b = W$. Equation 7 remains valid as the bed temperature changes with time providing the temperature profile remains uniform throughout the bed.

The solution is

$$h_c=\left[\left(h_b+\frac{R}{\delta}\right)^2-2d\left(W+\frac{R}{\delta}\right)+d^2\right]^{0.5}-\frac{R}{\delta} \tag{8}$$

At $h_c = 0$

$$\frac{H_b}{W}=-R^*+R^*\left\{1+\left(\frac{1}{R^*}\right)^2\left[2\frac{d}{W}(1+R^*)-\left(\frac{d}{W}\right)^2\right]\right\}^{0.5} \tag{9}$$

where H_b is the value of h_b at $h_c = 0$, and $R^* = R/\delta W$.

It can be seen that

$$\frac{d}{W}<\frac{H_b}{W}<\left[\frac{d}{W}\left(2-\frac{d}{W}\right)\right]^{0.5} \tag{10}$$

with the maximum value of H_b/W occurring at $R^* = 0$ (or $R = 0$) and the minimum value as $R^* \to \infty$.

Using Eq. 9, computations of H_b/W were made for $d/W = 0.03$, 0.1, and 0.3. These results are shown in Figure 3. For instance, if $R^* = 0.3$ and $d/W = 0.1$, then $H_b/W = 0.3$ and the channel has grown to nearly three times its initial depth. Conversely, if R^* is large, then $H_b/W \approx d/W$, with virtually no channel growth taking place. Interestingly, in fluidized beds the distributor resistance must also be selected to give uniform flow through the bed, and researchers have suggested that the ratio of plate-to-bed resistance should be greater than approximately 0.15 to 0.25. (Siegel, 1976; Kunii and Levenspiel, 1969). Of course, spatial instabilities are but one factor to be considered in choosing R^*; overall pressure drop, regeneration frequency, and stress level are also influenced by the choice of R^*.

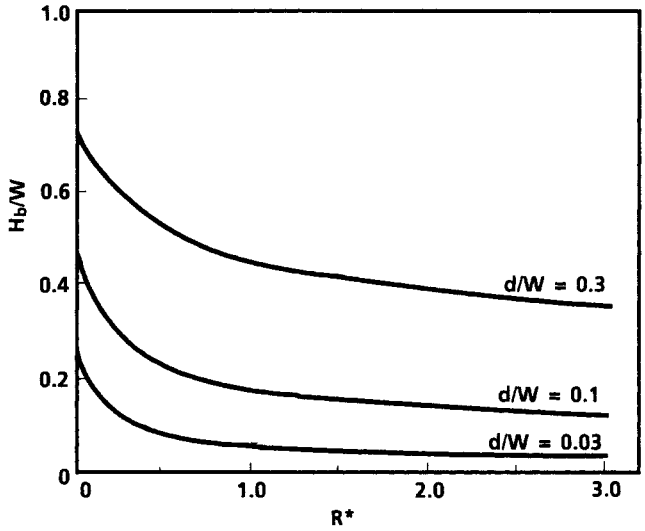

Figure 3. Dimensionless bed height when channel has completed regeneration.

Numerical Model of Channel Growth

In this section a simple numerical model is presented to examine spatial instabilities that occur throughout the regeneration cycle, that is, in both the kinetic and transport-controlled regimes. In the kinetic regime, the difference between bed and channel temperatures may be significant. Rather than solve a two-dimensional moving boundary problem, two special cases were considered using a quasi one-dimensional model:

1. An isothermal case, with bed and channel temperatures equal, but no mass transfer between bed and channel.
2. An adiabatic case, where the bed and channel temperatures are not equal and no heat or mass transfer occurs between bed and channel.

Similar planar cases have been considered by previous researchers in other regeneration models (Bissett and Shadman, 1985; Wiedemann et al., 1983, 1984). Once again, we used average values of velocity and temperature in the direction normal to the wall.

These models are straightforward extensions of the model of Bissett and Shadman. Assuming the solid and gas-phase temperatures were equal in the bed, they wrote the equations of change for bed temperature and height during regeneration as:

$$\frac{d\bar{T}}{d\bar{t}}=\frac{\bar{F}(\bar{t})}{\bar{C}_{ps}\bar{h}+\bar{C}_{pp}\bar{W}_p}\cdot\left(\Delta\bar{H}y_i(\bar{t})\left\{1-\exp\left[-\frac{\bar{k}(\bar{T})\bar{h}}{\bar{T}\bar{F}(\bar{t})}\right]\right\}+\bar{T}_i(\bar{t})-\bar{T}\right) \tag{11}$$

$$\frac{d\bar{h}}{dt}=-\bar{M}\bar{F}(\bar{t})y_i(\bar{t})\left\{1-\exp\left[-\frac{\bar{k}(\bar{T})\bar{h}}{\bar{T}\bar{F}(\bar{t})}\right]\right\} \tag{12}$$

The notation is similar to that of Bissett and Shadman (1985) with all variables nondimensionalized (see the Notation section.) Equation 11 is derived from an energy balance about a

control volume consisting of the bed and porous plate. The equation describes the energy convected in and out of the control volume, the heat generated by the reaction, and the energy stored within the volume. Equation 12 follows from Eq. 1 by substituting the value for y_e determined from a quasisteady species balance on y, assuming a first-order oxidation of carbon. The initial conditions are $\overline{T} = \overline{h}(0) = 1$.

The dimensional form of the reaction rate function, $k(T)$, is given by:

$$k = k_o T \exp(-E/R_g T) \tag{13}$$

In the present calculations we assume that Eqs. 11 and 12 can be applied separately to the bed and channel regions. For the isothermal case, the temperature is the same in the two regions (but varies in time), yielding three equations that must be solved. For the adiabatic case, T_b is not equal to T_c, and four equations are solved. In both cases, the channel and bed gas velocities are calculated from Eqs. 5 and 7, modified to account for the viscosity change as a function of temperature, using the power law relation (Bird et al., 1960). That is, δ and R in Eq. 6 are written as $\delta = \delta(T)$, $R = R(T)$.

Note that two-dimensional effects are neglected in this formulation. Combustion along the vertical sides of the channel is neglected, which will cause the channel to widen with time. Heat conduction in front of the channel should be enhanced by the bunching of isotherms and promote channel growth, similar to instabilities seen in crystal growth (Mullins and Sekerka, 1963). Similarly, the details of the gas flow field, both upstream of the interface and within the bed, can influence the growth rate (Miller, 1975). In the present calculations we neglect these effects, focusing instead on illustrating the interaction between the kinetic and transport instability mechanisms.

To aid in interpreting the results, we will consider the ratio of differential change in channel to bed height, derived from Eq. 12 in dimensional form:

$$\frac{dh_c}{dh_b} = \frac{u_c}{u_b}\left\{\frac{1 - \exp\left[-\dfrac{k(T_c)h_c}{T_c\beta u_c}\right]}{1 - \exp\left[-\dfrac{k(T_b)h_b}{T_b\beta u_b}\right]}\right\} \tag{14}$$

The righthand side of Eq. 14 consists of two multiplicative terms; the first is the ratio of transport terms, the second is the ratio of kinetic terms. These ratios are discussed later.

Numerical Results

The equations for each case were solved by a Runge-Kutta-Gill routine, and solutions were verified to be independent of the time step. Parametric values (tabulated in the Notation under each variable name), including $T_i(t)$, were taken from Bissett and Shadman (1985). A planar regeneration solution produced results that agreed with those of Bissett and Shadman.

Since a one-dimensional analysis cannot give information about the shape of the channel as it evolves, or determine the most rapidly growing wavelength, we must simply postulate the channel width parameter, α. Initially we consider wide channels, with $\alpha = 0.5$, which will tend to slightly minimize the effect of the transport instability. Later, narrow channels are considered.

Isothermal results

Results for the change in dimensionless channel depth, $(h_b - h_c)/W$, as a function of regeneration time are shown in Figure 4 with $\alpha = 0.5$ and $d/W = 0.1$. During the early stages the channel decreases slightly in depth until the end of the kinetic stage, which for $R^* = 0.1$ and 10 occurs at approximately 95 s. The channel decreases because the bed height is thicker than the channel, decreasing the kinetic ratio in Eq. 14. Once the kinetic stage ends in both the channel and bed, the kinetic ratio approaches unity and the regeneration rate is primarily governed by the transport ratio, u_c/u_b. Figure 5 shows that u_c is significantly greater than u_b for $R^* = 0.1$, and $u_c \approx u_b$ for $R^* = 10$. Consequently, for $R^* = 0.1$ the channel growth is large, and for $R^* = 10$ the channel growth is small.

These results can be compared to the isothermal results in Figure 3, which were generated with Eq. 9. Equation 9 applies only during the transport zone; consequently, Eq. 9 will predict H_b in Figure 4 providing that W and d are taken to be the bed height and channel depth at the end of the kinetic zone. Note that Figure 3 shows a greater H_b than Figure 4 because the kinetically driven recession of the bed is not included in Figure 3.

Adiabatic case—two competing instabilities

Figure 6 shows the dimensionless channel depth, $(h_b - h_c)/W$, as a function of regeneration time for three values of R^*: 10, 1, and 0.1, with $\alpha = 0.5$ and $d/W = 0.1$. Figure 7 shows the velocity in the channel and bed, while Figure 8 shows a representative plot of channel, bed, and filter-inlet gas temperatures.

As in the previous examples, the channel growth is ultimately small for $R^* > 1$. The kinetic stage, which exists from $t = 0$ to more than 90 s for both $R^* = 0.1$ and 10, dominates the channel growth for $R^* = 10$, and the bed completes regeneration before the channel. Here the bed burns fastest due to the higher initial height and overtakes the channel at about 92 s, driving the channel depth negative. The large R^*, and consequently nearly equal

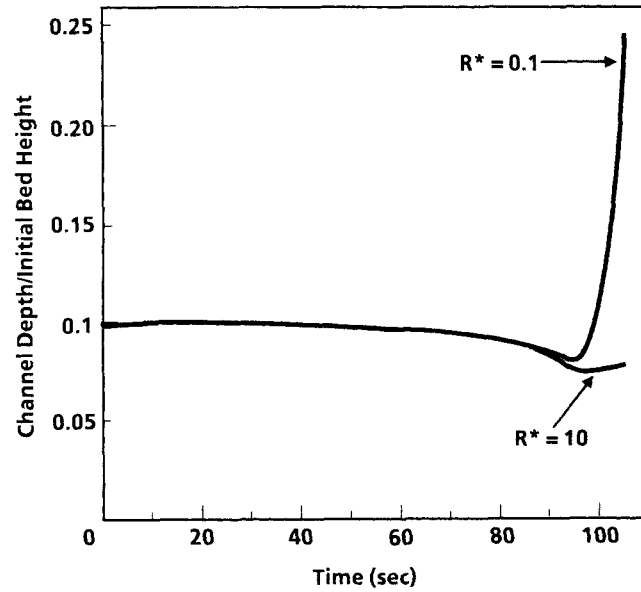

Figure 4. Channel depth as a function of regeneration time for equal bed and channel temperatures.
Two values of flow resistance parameter R^* are shown

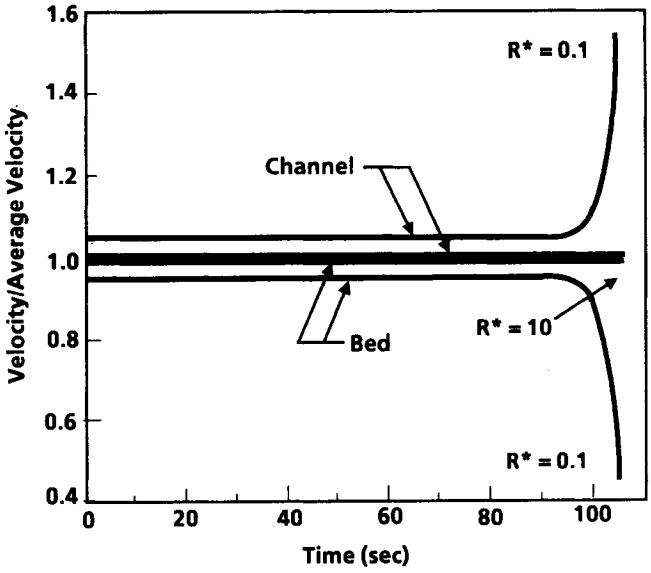

Figure 5. Gas velocity through channel and surrounding bed as a function of time and flow resistance parameter for equal bed and channel temperatures.

u_c and u_b, keep the transport instability from increasing the channel growth. At $R^* = 0.1$, channel growth is ultimately large because of the high ratio of u_c to u_b, but the growth is not as large as the isothermal case because of the offsetting influence of the kinetic stage.

The curves of u_c and u_b, Figure 7, are similar to the isothermal case, Figure 5, except for the behavior near the end of the kinetic stage. For $R^* = 0.1$, u_c/u_b is nearly a constant until $t > 90$ s, when the channel depth begins to significantly decrease. Flow then increases through the bed until the kinetic zone ends at $t \approx$ 95 s. After this, u_c/u_b gets large as the channel deepens due to transport effects. For $R^* = 10$, $u_c \approx u_b$ until the bed and channel heights are approximately equal. At this point, differences in viscosity become significant enough to cause u_c/u_b to change slightly.

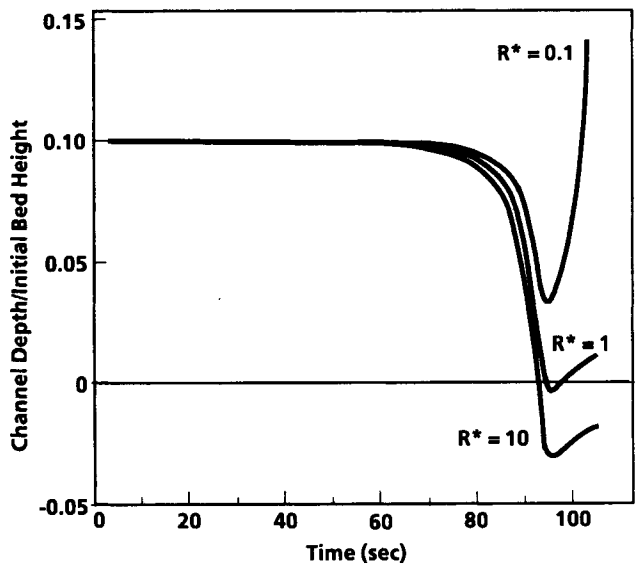

Figure 6. Channel depth as a function of regeneration time for unequal bed and channel temperatures.
Three values of flow resistance parameter R^* are shown

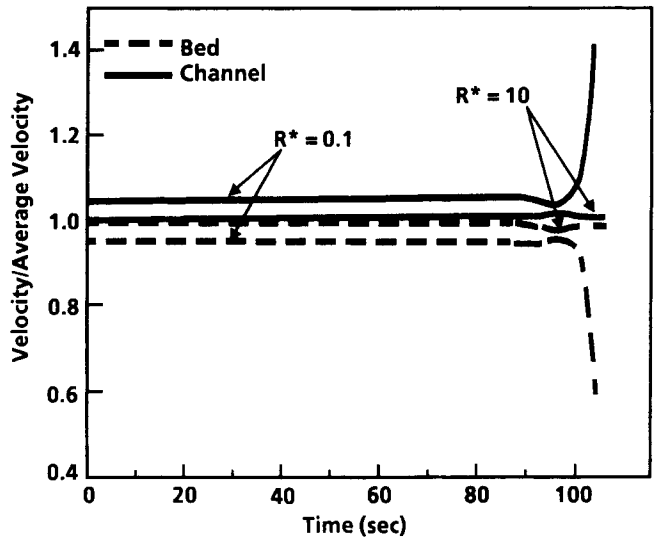

Figure 7. Gas velocity through channel and surrounding bed for unequal bed and channel temperatures.

Figure 8 shows bed, channel and inlet gas temperatures for an intermediate case, $R^* = 1$, which are generally representative of the behavior at other values of R^*. That is, the channel temperature was only insignificantly hotter than the bed temperature at early times. Although it cannot be resolved in the figure, the channel is slightly hotter than the bed because the gas heats the channel faster since $u_c > u_b$. This occurs until about 80 s, when T_c and T_b overtake T_i and the entering gas then cools the bed and channel. Ultimately, T_b becomes 25 to 40 K hotter than T_c. For $R^* = 0.1$, the channel temperature follows the same pattern,

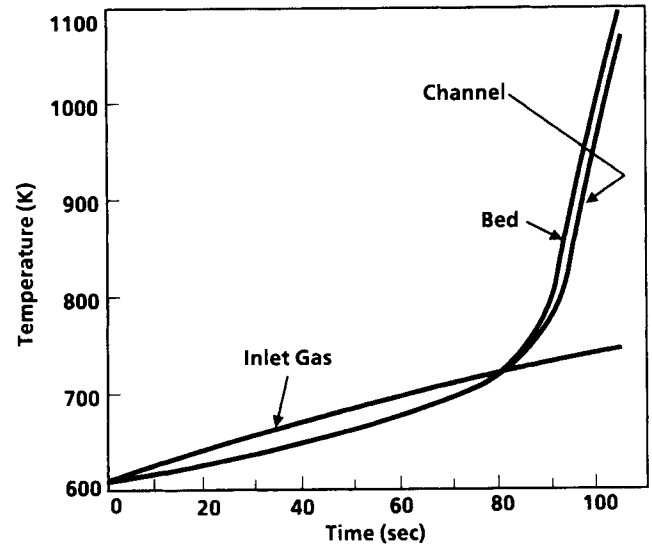

Figure 8. Channel, surrounding bed, and inlet gas temperatures as a function of time for $R^* = 1$.

except at the latter part of the transport stage when T_c overtakes T_b. This temperature difference rises to just over 30 K when h_c = 0.

It is useful to consider Eq. 14 for the adiabatic cases. Figures 9 and 10 show the transport and kinetic ratios from Eq. 15 and dh_c/dh_b for R^* = 10 and 0.1, respectively. With R^* = 10, dh_c/dh_b follows the kinetic ratio, since the $u_c/u_b \approx 1$. The bed overtakes the channel primarily because of the influence of height and temperature differences on the kinetic ratio. At the end of the kinetic stage dh_c/dh_b changes abruptly and follows the transport curve.

When R^* = 0.1 the transport ratio has a significant influence even during the kinetic stage. Initially dh_c/dh_b follows the shape of the kinetic ratio curve but is displaced from it due to the transport effects. This occurs until approximately 95 s, when dh_c/dh_b starts to follow the transport ratio curve. Note that the kinetic term has a concave downward shape in the kinetic stage. This is because the higher gas velocity in the channel results in a slightly faster heatup of the channel, increasing the kinetic influence for $t < 50$ s. For $t > 50$ s, this effect is offset by the difference in height between the channel and surrounding bed. Gradually the bed becomes significantly hotter than the channel and this, coupled with the bed height, decreases the kinetic ratio further.

There is actually a second kinetic stage just before regeneration is completed, when h becomes sufficiently less than the characteristic reaction zone thickness. Since in these cases the reaction zone is very thin and the bed height is negligibly small, it is not shown on the figures or explored further.

In the previous computations the ultimate channel growth has been less than the growth in the isothermal cases because of the offsetting influence of the kinetic stage. Next we seek the more detrimental conditions where the kinetic and transport-controlled growth act together and result in significantly larger channel growth and hence, higher thermal stresses. Since these conditions are of the most concern to the designer, we illustrate

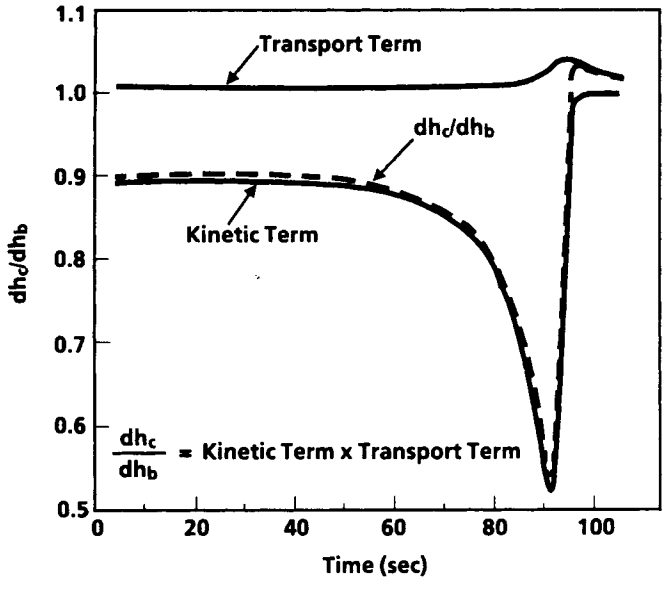

Figure 9. Ratio of channel to surrounding bed growth rates for R^* = 10.
Kinetic and transport terms are defined in Eq. 14

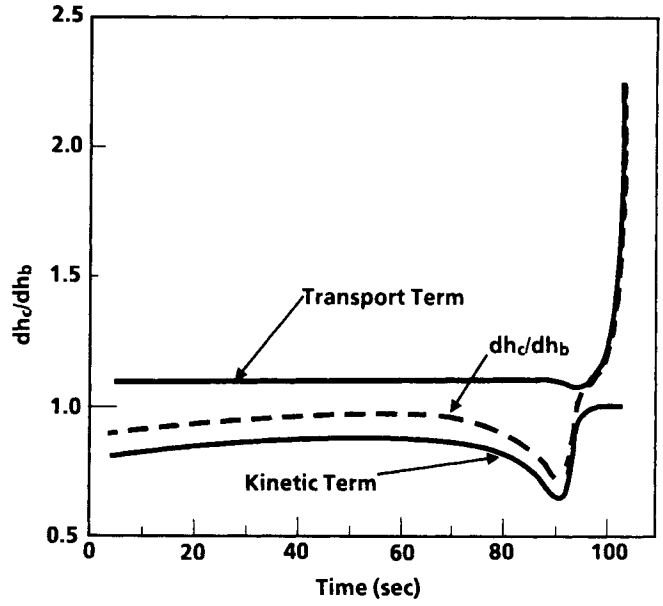

Figure 10. Ratio of channel to surrounding bed growth rates for R^* = 0.1.
Kinetic and transport terms are defined in Eq. 14

the phenomena by varying two design parameters: the average gas velocity entering the trap, u, and the slope of the exhaust gas temperature as a function of time, $T_f(t)$. In addition we consider narrow channels with α = 0.1.

The slope of the exhaust gas temperature-time curve was changed by varying the linear coefficient, a_1, in a polynomial representation:

$$T_f = a0 + a_1 t + a_2 t^2 \qquad (15)$$

For the base case, shown in Figure 6, a_0 = 606, a_1 = 1.7583, a_2 = 0.003958.

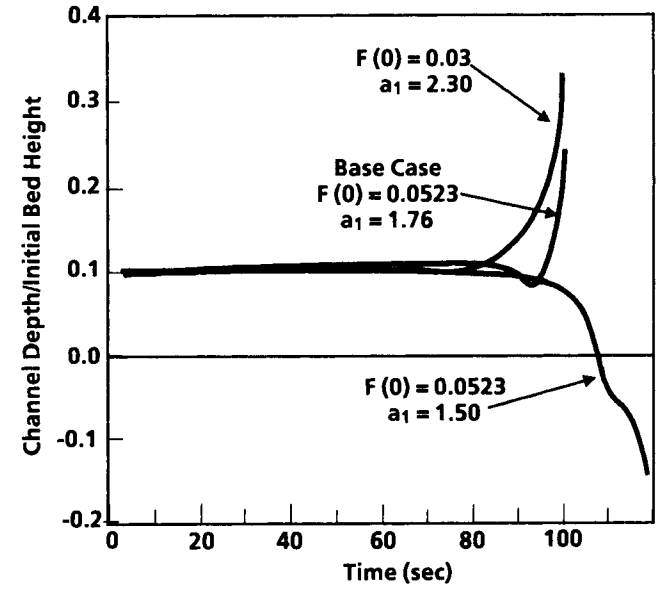

Figure 11. Channel depth for three cases with α = 0.1 and R^* = 0.1.

Results are shown in Figure 11. The base case, but now with $\alpha = 0.1$, is the middle curve and shows a moderately deeper channel at completion compared to Figure 6. However, the upper curve shows a significantly deeper channel than the previous adiabatic cases. The lower curve shows that the transport and kinetic instabilities can combine to let the bed complete regeneration much earlier than the channel.

In the upper curve the exhaust gas mass flow was reduced to 0.03 kg/s from the base case value of 0.0523 kg/s and a_1 was increased to 2.3. Consequently the exhaust gas heated the channel more than the surrounding bed throughout the kinetic stage and forced the channel to grow faster than the bed throughout the entire regeneration process.

In the lower curve the exhaust gas flow was held at 0.0523 kg/s but a_1 was decreased to 1.5. This reduced the heating of the channel by the gas. The larger height of the bed and the temperature difference resulted in such a high bed regeneration rate that the bed height was significantly less than that of the channel at the end of the kinetic stage. Consequently the transport-controlled growth was higher in the surrounding bed than the channel, and the bed completed regeneration well before the channel.

Conclusions

The results of simple mathematical models lead us to suggest that both transport and kinetic instability mechanisms are important and that significant thermal gradients in the wall are possible due to these spatial instabilities. We have shown that in some cases a small depression in the bed surface is unstable due to transport effects and finishes regeneration before the surrounding bed, while in other cases the bed completes regeneration before the depressed area. For certain combinations of gas velocity and temperature history, the kinetic and transport growth act together, resulting in highly nonuniform regeneration and larger thermal stresses in the monolith wall.

Channel growth by the transport mechanism can be reduced by increasing the parameter R^*, which is defined as the ratio of wall-flow resistance to soot-bed flow resistance. Since the kinetic mechanism can either offset or add to channel growth by the transport mechanism, an optimal design should seek to reduce the growth of all instabilities. Sufficient lateral heat transfer within the bed and wall, and judicious selection of exhaust gas velocity and temperature history should reduce the growth of kinetically driven instabilities and the coupling of kinetic and transport instabilities, although this remains to be experimentally demonstrated.

Acknowledgment

This work was initiated while the author was at Brookhaven National Laboratory. Discussions with C. R. Krishna and Robert McGraw are gratefully acknowledged.

Notation

Parameter values in parentheses and notation are generally taken from Bisset and Shadman (1985).

A = area of filter (1.63 m^2)
C_{pg} = heat capacity of exhaust gas (1.09×10^3 J/kg · K)
C_{pp} = heat capacity of porous plate (1.11×10^3 J/kg · K)
$\overline{C}_{pp} = C_{pp}\rho_p/(C_{pg}\rho)$
C_{ps} = heat capacity of bed (1.51×10^3 J/kg · K)
$\overline{C}_{ps} = C_{ps}\rho_s/(C_{pp}\rho)$
d = initial channel depth, m
E/R_g = activation energy/gas constant (1.8×10^4 K)
f = soot deposition flux, kg/m^2 · s
$\overline{F}$ = dimensionless gas mass flow rate, $F/F(0)$
$F(0)$ = initial mass flow rate of gas (5.23×10^{-2} kg/s)
h = thickness of soot bed, m
h_c = thickness of bed at channel, m
h_b = thickness of bed surrounding channel, m
h_g = thickness of porous plate, m
$\overline{h}$ = dimensionless bed height, h/W
H_b = h_b when $h_c = 0$, m
ΔH = heat of reaction (3.93×10^8 J/kmol)
$\overline{\Delta H}$ = heat of reaction $\Delta H/C_{pg}TM_a$
k = defined by Eq. 13
k_0 = reaction rate constant (596 m/s · K)
$k = sWAPM_ak/[R_gT_0F(0)]$
M_c = atomic weight of carbon deposit (12.0 kg/kmol)
M_a = molecular weight of exhaust gas (29.0 kg/kmol)
$\overline{M} = M_c/M_a$
P = gas pressure (101 kPa)
$R^* = R/\delta W$
R = flow resistance of porous plate, Eq. 2
R_g = gas constant (8.31 m^3 kPa/kmol · K)
s = specific surface area of bed (5.5×10^7 m^{-1})
t = time since beginning of regeneration cycle, s
$\overline{t}$ = dimensionless time, ut/W
T = soot layer temperature, K
$\overline{T}$ = dimensionless soot layer temperature, T/T_0
T_i = exhaust gas temperature entering the filter, K
$\overline{T}_i = T_i/T_0$
T_0 = gas reference temperature, K
u_b = gas velocity in bed surrounding channel, m/s
u_c = gas velocity in channel, m/s
u = average gas velocity, m/s
W = initial bed thickness, m
W_p = thickness of porous plate (4.32×10^{-4} m)
y_e = mole fraction of oxygen exiting bed
y_i = mole fraction of oxygen entering bed (0.052)
y = mole fraction of oxygen in bed

Greek letters

α = fraction of cross-sectional bed area occupied by channel
$\beta = \rho R_g/SPM_a$
ΔP = pressure drop through bed and porous plate
δ = bed flow resistance coefficient, Eq. 2
ρ = gas-phase density
ρ_b = solid-phase bulk density (5.5×10^2 kg/m^3)
ρ_p = porous plate bulk density (1.4×10^3 kg/m^3)
μ = exhaust gas viscosity

Subscripts

b = bed
c = channel
overbar = dimensionless quantity

Literature Cited

Bird, R. B., W. E. Stewart, and E. N. Lightfoot, *Transport Phenomena*, Wiley, New York (1960).

Bissett, E. J., "Mathematical Model of the Thermal Regeneration of a Wall-Flow Monolith Diesel Particulate Filter," *Chem. Eng. Sci.*, **39**, 1233 (1984).

Bissett, E. J., and F. Shadman, "Thermal Regeneration of Diesel-Particulate Monolithic Filters," *AIChE J.*, **31**, (5), 753 (1985).

Grossman, G. "Melting, Freezing, and Channeling Phenomena in Ice Counterwashers," *AIChE J.*, **22** (6), 1033, (1976).

Kunii, D., and O. Levenspiel, *Fluidization Engineering*, Wiley, New York (1969).

Langer, J. S.,"Instabilities and Pattern Formation in Crystal Growth," *Rev. Mod. Phys.*, **52** (1), 1 (1980).

MacDonald, J. S., and G. M. Simon, "Development of a Particulate Trap System for a Heavy-Duty Diesel Engine," SAE Paper No. 880006 (1988).

McGraw, R., and J. Wegrzyn, "Morphological Stability in the Restricted Model of a Burning Spherical Particle," 16th Ann. Meet. Fine Particle Soc. Miami Beach, April 22–26 (1985).

Miller, C. A., "Stability of Moving Surfaces in Fluid Systems with Heat and Mass Transport. III: Stability of Displacement Fronts in Porous Media," *AIChE J.*, **21**(3), 474 (1975).

Montierth, M. R., "Fuel Additive Effect upon Diesel Particulate Filters," SAE Paper No. 840072 (1984).

Mullins, W. W., and R. F. Sekerka, "Morphological Stability of a Particle Growing by Diffusion or Heat Flow," *J. Appl. Phys.*, **34**(2), 323 (1963).

Siegel, R., "Effect of Distributor Plate-to-Bed Resistance Ratio on Onset of Fluidized-Bed Channeling," *AIChE J.*, **22**(3), 590 (1976).

Wade, W. R., J. E. White, J. J. Florek, and H. A. Cikanek, "Thermal and Catalytic Regeneration of Diesel Particulate Traps," SAE Paper No. 830083 (1983).

Wiedemann, B., U. Doerges, W. Engeler, and B. Poettner, "Regeneration of Particulate Filters at Low Temperatures," SAE Paper No. 830086 (1983).

———, "Application of Particulate Traps and Fuel Additives for Reduction of Exhaust Emission," SAE Paper No. 840078 (1984).

Manuscript received Dec. 13, 1988, and revision received Dec. 14, 1989.